Reservoir regime and controls in the Karaha-Telaga Bodas Geothermal Field, Indonesia.

Michal Nemčok[1], Joseph N. Moore[1], Chelsea Christensen[1], Rick Allis[2], Thomas Powell[3], Brad Murray[4], Greg Nash[1], and Jess McCulloch[5]

[1]Energy & Geoscience Institute, 423 Wakara Way, Suite 300, Salt Lake City, UT 84108
[2]Utah Geological Survey, 1594 W North Temple Street, Suite 3110, Salt Lake City, UT 84116, USA
[3]Thermochem, Inc., 3414 Regional Parkway, Suite A, Santa Rosa, CA 95403, USA
[4]Department of Geology and Geophysics, University of Utah, 135 S. 1460 E., RM 719 Salt Lake City, UT 84112-0111
[5]Coso Operating Company, LLC, 900 N. Heritage Drive, Ridgecrest, CA 93555

Keywords
Stress, pressure, fracture, reservoir, seal, rheology, geothermal

Abstract

1. Introduction

The Karaha-Telaga Bodas geothermal field hosts high temperature reservoir with liquid- and vapor-dominated zones on the flank of Galunggung Volcano in West Java (Allis et al., 2000) (**Fig. 1a, b**). The field is hosted by stratovolcanic andesitic suite expressed in topography as a N-S trending ridge with volcano close to its southern end. The ridge is perpendicular to the modern-day minimum principal stress (Nemčok et al., 2001). The heat for the system is supplied by a granodiorite dyke, which is roughly parallel to the ridge at a depth of 1-3 km (Allis et al., 2000). The system consists of a cap rock, which is from several couple hundred meters to 1600 m thick, characterized by steep temperature gradients and low permeability, an underlying vapor-dominated zone that extends to depths below the sea level, and a deep liquid-dominated zone with measured temperatures up to 350° C (Allis et al., 2000). Large-scale faults in the field have the following orientations (**Fig. 1b**): dip directions of 90-120° and 270-300° for normal faults, 20-40° and 200-220° for dextral strike-slip faults, 40-60° and 220-240° for dextral slightly oblique-slip faults, 60-90° and 240-270° for dextral oblique -slip faults, 120-130° and 300-310° for sinistral oblique-slip faults and 130-150° and 310-330° for sinistral strike-slip faults.

Data from the field: fracture logs from coreholes, interpretations of Electrical Micro Imaging (EMI) and Formation Micro Scanner (FMS) images from wells, pressure and temperature measurements from deep exploration and core holes, and results of mineralogical, petrological and geochemical analyzes, provide a unique opportunity to characterize both regime and controls of the high temperature liquid-vapor system.

Individual goals include:

- determination of how does the rock strength control the top and bottom of the fractured reservoir;
- determination of how does the stress control the top and bottom of the fractured reservoir;
- determination of how does the alteration and cementation control the top of the fractured reservoir;
- determination of what controls production zones;
- determination of what controls the presence of the liquid-vapor system in the reservoir.

2. Methods

FMS, EMI images from two wells KRH 3-1 ST and KRH 2-1 OH with interpreted fracture and bedding plane tadpole diagrams were provided by the Karaha-Bodas Company, LLC, as well as pressure/temperature (pT) and lithological logs for all wells **(Fig. 2a)**.

The original work includes detailed lithology and fracture logging from coreholes K-21, K-33, T-2 and T-8 and microscopic study of cuttings from remaining wells. Meso-scale and micro-scale logging focused on determination of mineralization events in both host rocks and fractures. Lithological data were combined with temperature logs to calculate strength distributions within the wells using the relationship (Ranalli and Murphy, 1987):

$$(\sigma_1 - \sigma_3) = \beta\rho g z(1 - \lambda), \qquad (1)$$

where σ_1 and σ_3 are maximum and minimum principal compressional stresses, β is a constant (3 for thrusting, 1.2 for strike-slip faulting and 0.75 for normal faulting), ρ is the rock density, g is the acceleration of gravity, z is the depth and λ is the hydrostatic/lithostatic pressure ratio. The smaller of calculated brittle and ductile strengths was taken as controlling the rock column. Most of the wells did not penetrate deep enough to reach the ductile zone, and, therefore, were extended downward using interpreted lithologies from gravity and magnetotelluric studies (Tripp et al., 2002, Joe adds MT reference) to reach the depths at least about 2 km below the sea level.

Fracture data from wells KRH 3-1 ST and KRH 2-1 OH were used for calculation of normal and shear stresses at fracture walls using in situ stress data from the reservoir. They were used for fracture slip vector and displacement determination. The slip tendency for each fracture was calculated from the relationship:

$$\tau/\sigma_n \qquad (2)$$

The dilation tendency is given by:

$$(\sigma_1 - \sigma_n)/(\sigma_1 - \sigma_3), \qquad (3)$$

where σ_1 is the maximum principal compressive stress, σ_3 is the minimum principal compressive stress, τ is the shear stress and σ_n is the normal stress (**Tab. 1**). Normal stresses acting upon fractures were compared to a compressional strength of the wall rock (**Tab. 2**).

Calculated fracture kinematics from wells KRH 3-1 ST and KRH 2-1 OH were used to interpret Landsat-7 Thematic Mapper™ data, captured on August 30, 1999. Interpreted fault-topographic surface intersections were assigned most likely dip intervals and, using this dip constraint, linked with faults determined in subsurface, using software Petrel.

A three-dimensional geologic model of the field in Petrel was made containing mentioned faults, temperature surface maps (**Fig. 2b**) made from temperature logs from wells, and mineral distribution contour maps made from core logging and microscopic data. The minor and major lost circulation zones recognized in wells during drilling were located in the Petrel model and compared to our fracture/stress and mineralogical data at these locations.

Liquids and gases discharged from wells were subjected to chemical and isotopic analyses. Weirbox brine samples contaminated by drilling water were recalculated to their state at downhole conditions, using aquifer temperature chosen to match both the quartz and Na-K-Ca geothermometers (Powell et al., 2001). Various elemental distributions, such as 4 Rb-Li-10 Cs, 100 Li-Cl-25 B, and H_2S-10 CH_4-10 NH_3, were grouped in ternary diagrams in order to determine reservoir compartments. Binary diagrams of log H_2/log CO_2 and $\delta D/\delta^{18}O$ were made for the same purpose.

3. Data

3. 1. Temperature data

Temperature logs along wells indicate major differences in the heat transfer among various parts of the Karaha-Telaga Bodas geothermal field. Temperature log along well K-33 serves as an example documenting a more-or-less linear temperature increase with depth, dominated by conductive heat transfer, which is typical for shallower zone, roughly overlapping with a cap rock (**Fig. 2a**). Temperature regime in the deeper section indicates that the heat transfer is dominated by convection, where geothermal fluids maintain roughly the same temperature regime throughout the reservoir section. Reservoir temperature regime in well K-33 is perturbed by thermal effects of lost circulation zones, typically indicated by large and small temperature minima for major and minor fluid entries, respectively (**Fig. 2a**).

250° C temperature surface, typically used by geothermal industry as proxy for the top of the reservoir, indicates a thin cap rock section and a shallow top of the reservoir in the southern part of the field, Telaga Bodas area, and a thick cap rock section and a deep top of the reservoir in the northern part, Karaha area (**Fig. 2b**). In more detail, the central part of the field is characterized by a saddle in the top reservoir surface and the northernmost part of the field by a down plunging surface in northerly direction (**Fig. 2b**).

3. 2. Strength data

Temperature regime combined with rock rheology distribution controls the strength distribution, characterized by the upper brittle and lower ductile zone (**Fig. 3**). Brittle deformation zone overlaps with both cap rock and reservoir section, ductile zone underlies the reservoir. The boundary between brittle and ductile zones appears to be rather sharp, mimicking the temperature distribution.

3. 3. Electrical image and stress data at identified lost circulation zones controlled by fractures

Well KRH 2-1 OH serves as an example of "leaky" northern part of the field, the Karaha area, where lost circulation zones were observed not only in the reservoir section but also in the cap rock (**Fig. 4a**). Similar evidences come from neighbor wells such as KRH 1-1, KRH 4-1, KRH 5-1 and K-10, while wells in the southern part of the field, the Telaga Bodas area, such as TLG 1-1 and TLG 2-1, contain lost circulation zones only in the reservoir section.

Three and six of the minor fluid entry points in well KRH 2-1 OH were determined in lava and pyroclastic/epiclastic/tuff sections, respectively. The only major entry was observed in pyroclastic/epiclastic/tuff section (**Fig. 4a**). The FMS image of the minor fluid entry in pyroclastic/epiclastic/tuff section at a depth of 2032 m is shown in **Fig. 4b**. The involved rock section, which appears massive, has an overall electrically resistive appearance. It is deformed by a fault characterized by electrically conductive image with small scattered pieces with resistive image.

Example of the fracture-controlled major entry comes from well KRH 3-1 ST (**Fig. 4c**). Three fractures with electrically conductive image are cut in the massive rock section with combined resistive/conductive image. Examples illustrated by **Figs 4b** and **c** characterize most of the lost circulation zones in the field with exception of few fluid entries described later.

Calculated slip and dilation tendencies How of fractures from the field indicate that ? some of them are critically stressed, on a verge of reactivation, thus, determining the strength of the rock section where they are located (**Tab. 1**). Other regions indicate that their fractures are far from being critically stressed. Lower portion of the reservoir contains fractures, which are loaded by normal stresses larger than a compressional strength of the host rock, indicating that their asperities that would hold them slightly open are crushed and fractures most likely closed (**Tab. 2**). Two depth intervals with fractures from wells KHR 3-1 ST and KRH 2-1 OH (**Tab. 2a and b**) indicate that the magnitude of the loading normal stress depends on fracture strike and dip, thus forming a fuzzy boundary between open and closed fractures.

Certain trends in fracture/stress distribution characterize also the top of the reservoir, at least in the well K-33 (**Tab. 3**). Fracture log from corehole K-33 indicates that the cap rock section is deformed by a variety of fracture kinematic types while the reservoir contains almost exclusively only tensile fractures and normal faults (**Tab. 3**).

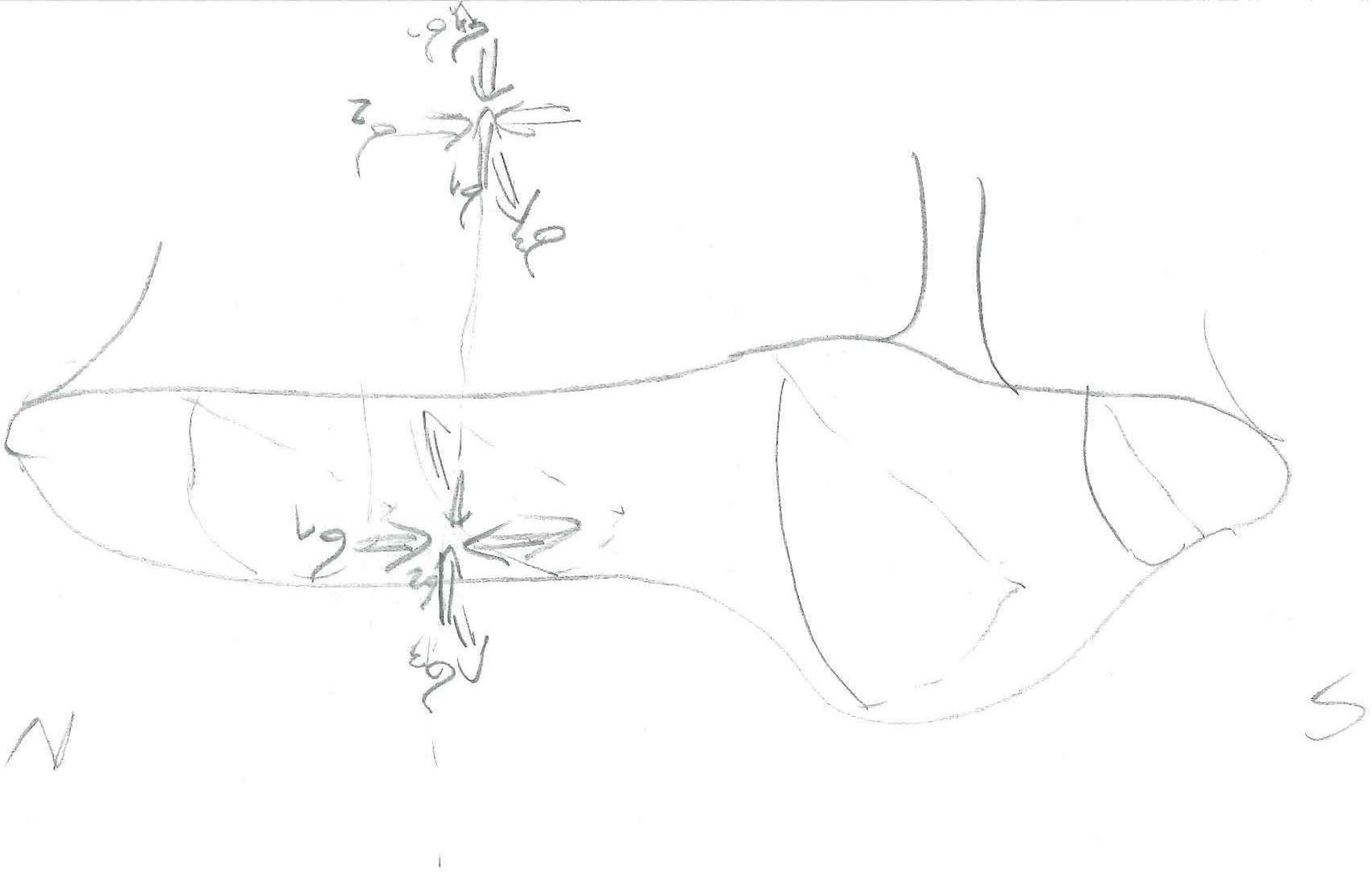σ3
σ2
σ1
σ1
σ1
σ2
σ3
N
S

3. 4. Alteration and cementation data

Top surfaces of different mineral distributions are frequently approximately parallel to the present-day isotherms (**Fig. 5b**) and to the top surface of the quartz diorite intrusion beneath the volcanic rocks. They are result of numerous mineralization events, which can be grouped into the three main groups (**Tab. 4**). The grouping is based on the mineral growth time relationships determined by optical (**Fig. 5a**), electronic scanning microscope studies (**Fig. 6b**) and meso-scale core logging (**Fig. 6a**).

The heat source for the field, quartz diorite intrusion, apparently forms a N-S striking large dyke, as suggested by the location of the topographic ridge right above it (**Fig. 1b**), and by the fact that wells located to the east and west of the N-S axis of the dyke indicate that the andesite/quartz diorite contact dips down considerably over short distances in eastward and westward directions. The dyke determination is in accordance with preliminary gravity model (Trip et al., 2002), which does not allow to choose an interpretation of the intrusion from a dyke and a narrow sill interpretations, and in accordance with the regional extension of a strike of 98° (Nemčok et al., 2001) being roughly perpendicular to its strike.

The temperature and mineral distributions (**Fig. 2b, 5b**) indicate that the feeder for the dyke was located below Telaga Bodas. The feeder is characterized by significant present-day flux of magmatic gases. Both the vertical dimension and total volume of the quartz diorite body are largest at its feeder. This is also the region with the largest temperature gradient in the Karaha – Telaga Bodas geothermal field.

The cap rock of the geothermal field is characterized by penetrative argillic alteration. Detailed logging of the K-33 well indicates that the alteration did not affect finer-crystalline andesite lava flows. It affected intervening pyroclastic, epiclastic and tuff horizons, resulting in a significant reduction of their permeabilities. Most of low permeability lava flows in the cap rock penetrated by wells do not contain any fractures. Fracture fill minerals in the cap rock include sericite, chlorite, pyrite, calcite, hematite, various clay minerals, chalcedony, quartz, and anhydrite (**Tab. 4, Fig. 5c**). Fractures are usually fully cemented and if they contain any open cavities, they are usually not interconnected.

The reservoir is characterized by penetrative argillic alteration (**Fig. 5a**), which decreases its matrix permeability, and contains fractures that are either almost open or at least contain a large amount of interconnected cavities (**Fig. 5c**). Fracture fill minerals in the reservoir contain sericite (**Tab. 4**), chlorite (**Tab. 4**), epidote (**Fig. 5b, c**), pyrite (**Fig. 6a**), chalcedony (**Fig. 6b**), quartz (**Fig. 5a**), anhydrite (**Fig. 5c**), calcite (**Fig. 6a, b**), and wairakite (**Fig. 5c**).

3. 5. Electrical image and stress data at identified lost circulation zones controlled by rock matrix

Well KRH 2-1 OH contains two examples of fluid entry points in the reservoir where electric image does not indicate presence of any fractures (**Fig. 7a, b**). The image shows an electrically conductive layered rock with either electrically resistive (**Fig. 7a**) or conductive bedding planes (**Fig. 7b**). The rock can be epiclastic flow, tuff horizon or lacustrine sediment. The fluid flow at the lost circulation zone during drilling must have been caused by high matrix permeability of the rock, electrically conductive image of which would indicate a significant fluid saturation of the reservoir horizon.

3. 6. Reservoir character

The reservoir contains liquid and overlying steam zones (**Fig. 8a, b**) with most of lost circulation zones recognized in the liquid reservoir (**Fig. 8a**). Pressure data indicate a single, liquid-reservoir pressure trend in northern and central parts of the field (Allis et al., 2000). The slope of the trend, 12mbar^{-1}, is to be expected from a fluid warmer than 200° C, which is in accordance with temperature data (**Fig. 8b**). A single pressure trend indicates a sufficient lateral reservoir communication to prevent compartmentalization. The elevation of the theoretical water surface at atmospheric pressure determined for the reservoir at more than 300 m above sea level is below the regional cold-water elevation (Allis et al., 2000).

Well KRH 4-2 from the NE part of the field, located on the flank of the Karaha – Telaga Bodas volcanic ridge, encountered higher liquid pressures, characterized by a head elevation of about 700 m above sea level. Well T-10 from the SW part of the field, located on the opposite flank of the ridge, had a head elevation of about 800 m above sea level (Allis et al., 2000). The valley floors on both sides of the ridge are at about 500 m above sea level, providing a minimum bracket for the head of the deep, liquid-saturated reservoir beneath flanks of the Karaha – Telaga Bodas volcanic ridge. The geothermal ? reservoir is under-pressured by at least 300 ± 100 m, i.e. 30 ± 10 bar.

The steam zone is under pressures of 55-65 bar, with highest pressures determined in the southern part of the field (Allis et al., 2000; **Fig. 8b**). The southern part is characterized by the thickening of the zone and its top reaching the surface (**Fig. 8b**). This area is characterized by variety of surface manifestations, such as fumaroles with associated argillic alteration, acidic Telaga Bodas lake, and chloride-sulfate-bicarbonate springs, some of which discharge moderate to low pH waters. The steam zone thins in direction towards the northern part of the field and its northern limit lies between wells KRH 2-1 and KRH 1-1 (**Fig. 8b**), without any proven connection to northern area with surface manifestations such as fumaroles and associated argillic alteration.

The flow in the liquid zone is towards the high-temperature vapor zone beneath the southern end of the system (**Fig. 8b**), with the dominant mass loss being the steam to the surface, and condensate outflow near-surface. Some lateral outflow and mixing of magmatic steam with low-salinity geothermal steam beneath the northern side of the southern part of the field cannot be ruled out (Allis et al., 2000). The magmatic vapor zone beneath the Telaga Bodas lake resembles a vapor chimney, surrounded by a condensate zone (**Fig. 8b**).

Although pressure data do not indicate any reservoir compartmentalization, chemical and isotopic data from liquids and gases indicate poor mixing (Powell et al., 2001). Chloride concentrations in various samples of reservoir fluids range from 1600 to 8000 ppm, chloride/boron ratios from 2.4 to 20 and Cl/Li and Cl/F ratios range over a an order of magnitude. Ternary plot of Rb, Li and Cs (**Figure 9a**) shows three clusters of distribution, so does the plot of Li, Cl and B (**Figure 9b**). The stable oxygen and hydrogen isotopes indicate two separate fluid trends in the liquid zone (Powell et al., 2001). Ternary plot of H_2S, CH_4 and NH_3 concentrations in various samples of reservoir gases shows three clusters of distribution (**Fig. 9c**).

4. Interpretation and discussion

4. 1. Rock strength control on the top and bottom of the fractured reservoir

The relationship between reservoir temperatures and rock distributions (**Fig. 8b**) suggests that the thermal regime in the geothermal field is controlled by the shape of the quartz diorite intrusion beneath the volcanic rocks, its cooling history, and the location of its shallow apex. The shape control can be implied from the rough parallelism of isotherms with the intrusion surface. **Figure 10b** indicates that isotherms in the ductile deformation zone conform to the intrusion surface. Top of the ductile zone is roughly parallel to adjacent isotherms and is subparallel to 330° C isotherm, since the brittle/ductile boundary lies inside the intrusive body, homogeneous at a large scale. Most of the quartz diorite intrusion is affected by ductile deformation regime. The only exception is a narrow external zone, which thickens towards the southern part of the field, and which undergoes brittle deformation. Overlying andesite stratovolcanic rock suite behaves in a brittle fashion.

The brittle/ductile boundary represents a maximum possible depth of the reservoir base, being a boundary between systems of interconnected shear and tensile brittle fractures above and lack of fractures below. Evidence for similar narrow brittle/ductile boundary comes from studies of ore deposits (e.g., Hedenquist et al., 1998; Fournier, 1999) from lacking fractures below this boundary, known from "bottoming out" of earthquakes (e.g., Gilpin and Lee, 1978; Majer and McEvilly, 1979; Sibson, 1982), and from geothermal wells drilled to depths with temperatures exceeding 370°-400° C (Cappetti et al., 1985; Ferrara et al., 1985; Fournier, 1981). All recognized lost circulation zones in the Karaha – Telaga Bodas geothermal field lie above the brittle/ductile boundary, the lowermost ones from wells TLG 1-1, TLG 2-1, TLG 3-1, KRH 1-1 and KRH 3-1 providing the closets proxies.

The minimum possible depth of the reservoir top is also controlled by mechanic stratigraphy. The cap rock initially consisted of permeable tuff horizons, pyroclastic and epiclastic flows intercalated with low permeability lava flows. The initial low permeability of lava flows can be implied from our logging of coreholes K-33 and K-21, which indicates that lava flows sandwiched among cap rock tuffs, epiclastics and pyroclastics were not affected by any significant alteration. Data from these two wells indicate that pyroclastics, epiclastics and tuffs were fair to good reservoir rocks prior to their alteration and compaction at the beginning of the development of the geothermal system (**Tab. 4, Fig. 5c**). However, penetrative shallow argillic alteration and later compaction progressively changed them into effective seals. Their penetrative deformation compared with no fracturing in sandwiched lava flows allows to conclude that the surrounding less competent horizons absorbed the deformation, allowing lava flows to escape fracturing and retain their initial sealing properties.

4. 2. Stress control on the top and bottom of the fractured reservoir

Fractured reservoir contains fracture clusters at various depth levels, which are characterized by different mineral parageneses. It is the lowermost fracture clusters, which are least cemented and most open, as documented by core logging in well K-33 (**Fig. 5c**). Therefore, it is generally the lowermost fracture clusters, which are typically weaker than surrounding reservoir rock. It is their strength that controls the overall reservoir strength in their area. Depending on their orientation to modern stress field, they can be reactivated or remain non-active or collapse (**Tab. 1**). Reacting to the local stress conditions, their fracture apertures can be increased, decreased, remain the same, or shut close (**Tab. 2**).

If we determine a fuzzy base of the reservoir by connecting the lowermost fractures, which did not become totally closed, having normal stresses resolved on fracture walls larger than compressional strength of the wall rock (see **Tab. 2**), we define a reservoir base, which lies above the brittle/ductile boundary. Normal faulting stress regime in the lower portion of the Karaha – Telaga Bodas reservoir causes shallow-dipping fractures to achieve closed state at shallower depths than steeply dipping fractures (**Tab. 5**). Steep fractures do not reach this state above the brittle/ductile boundary. Normal stresses of steeper fractures lower than compressional strength of the wall rock prevent their propping breccias and asperities from being crushed and their aperture from being closed.

Top of the reservoir is probably partly controlled by stress conditions, which, however, interact with more important mechanic stratigraphy and cementation. Fracture log from well K-33 indicates that central portion of the geothermal field can be characterized by the boundary between the overlying strike-slip stress regime and underlying extensional stress regime located roughly at the top reservoir level. It is indicated by presence of tensile and variety of shear fractures in the cap rock and presence of only normal faults and tensile fractures in the reservoir (**Tab. 3**). Because the central part of the field is characterized by a saddle in the top reservoir surface and maximum cap rock thickness (**Fig. 10a**), while the southern and northern parts by elevations on the top reservoir surface and reduced cap rock thickness, other parts of the field have upper reservoir portions controlled by strike-slip regimes.

Northern part of the field is also a region where in situ stresses keep some of the larger faults (see **Fig. 1b**) periodically reactivated. This controls thermal perturbations shown in **Fig. 10b** by a flow of warm fluids up these faults. A presence of leaky cap rock in this area is also documented by surface geothermal manifestations (**Fig. 10b**), occurrence of lost circulation zones inside the cap rock (**Fig. 8a**) and very steep temperature/depth distributions even in cap rock sections in some wells (**Fig. 4a**).

4. 3. Alteration and cementation controls on the top of the fractured reservoir

Apart from control on the cap rock mentioned earlier, alteration has the effect on various lithologies inside the reservoir. Pyroclastic flow at a depth of 1750.7 m in well K-33, for example, underwent penetrative feldspar dissolution and subsequent epidote cementation. The dissolution preferentially affected higher permeability clasts. Cavities after dissolved feldspars were just barely lined by epidote, which did not destroy an enhanced porosity. In this case the alteration effect on this reservoir area was permeability enhancement.

The example of the opposite effect comes from the deeper reservoir level of 1870.25 m in the same well. Here the lava flow underwent a penetrative dissolution that increased its porosity. This changed its deformational behavior from a very competent rock with tendency to dilate when fractured to a less competent rock with strain hardening behavior. Logged core is characterized by a several tens of cm wide zone of shear bands, which should act either as an effective seal or at least a baffle in the reservoir flow regime.

Both documented examples indicate that reservoir at Karaha – Telaga Bodas behaves as a system of fracture clusters, some of them permeable some of them not, inside of a mosaic of higher and lower permeability rock bodies.

Fracture permeability of this reservoir system ~~if~~ is further controlled by fracture cementation (**Tab. 4, 5a, c, 6a, b**). **Fig. 5c** indicates that one could expect different fracture fill in the fractures of the same orientations when occurring in different pressure/temperature conditions. One could further imply that different segments of the same fault would undergo different cementations. While some fracture cements have a tendency to clog fractures either by a complete fill (**Fig. 5a**) or by resulting in a system of not interconnected cavities (**Fig. 6b**), others just barely manage to line fracture walls (**Fig. 5c**; epidote, wairakite).

The most profound effect on pushing down the top reservoir surface was imposed by downward percolating condensates, resulting in precipitation of minerals such as anhydrite (**Fig. 5c**), calcite (**Fig. 6a, b**) and fluorite in response to increased temperature. **Figure 6a** from reservoir penetrated by well K-33 shows how a small-scale normal fault with earlier pyrite cement located in dilatant jogs with remaining open spaces became completely sealed by subsequent calcite precipitation. Similar effect with less complete clogging is documented from reservoir levels in well T-2, where calcite took on open cavities left after chalcedony/quartz precipitation (**Fig. 6b**). Different cementation stage of fractures of different location and orientation results in a fuzzy top surface of the fracture reservoir.

4. 4. Production zone controls

Comparison of **Figures 4b** and **4c** with **7a** and **7b** documents that reservoir in the Karaha – Telaga Bodas geothermal field contains both fracture and matrix permeability systems. Fracture-controlled lost circulation zones studied in wells KRH 2-1 OH and KRH 3-1 ST were located in massive brittle andesitic rocks. Matrix-controlled lost circulation zones were located in porous tuff, epiclastic and lacustrine sediment horizons.

Matrix-controlled minor fluid entries in well KRH 2-1 OH are shown in **Fig. 7a** and **7b**. Their electrically conductive FMS rock images indicate an increased saturation by electrically-conductive fluid, which adds to the resistive image of the rock skeleton.

There are no fractures imaged in both figures, indicating that the only permeability is the matrix permeability, perhaps enhanced by some permeability along bedding planes, as indicated by several bedding planes with electrically-conductive image.

Two more matrix-controlled fluid entries were determined in the well KRH 3-1 ST at depths of 2306.5 m and 2381. 5 m. Their EMI images lack any fractures. Moderately electrically conductive images of their host rock indicate an increased fluid content in their otherwise resistive rock skeleton. The thickness of layered sequence hosting the fluid entry at 2381.5 m is 126 m, which is a value comparable with acceptable thickness of producing hydrocarbon reservoir horizon. Detailed fracture logging indicates that the whole horizon contains just 17 minor fractures and its fracture density is just 1.3 fractures per 10 m in comparison to 5-10 fractures per 10 m characteristic for lava flows. The thickness of layered sequence hosting the fluid entry at 2306.5 m is only 12.2 m. It contains only 1 minor fracture.

All studied matrix-controlled fluid entries are in layered rock sequences with fracture densities well below the density of fractures in massive volcanic sequences dominated by lava and pyroclastic flows.

Fracture-controlled fluid entries in wells KRH 2-1 OH and KRH 3-1 ST are shown in **Fig. 4b** and **4c**, respectively. **Fig. 4c** shows the major fluid entry at a depth of 2827.5 m in well KRH 3-1 ST, containing three fractures that control its permeability. When we compare their EMI image with images of non-productive fractures in the same well, it turns out that non-productive fractures are frequently lined by resistive zones, indicating continuous cementation by resistive minerals such as calcite or quartz, as documented by fracture logging of coreholes K-33 and K-21. Fracture apertures are usually at the threshold of the recognition of the method, i.e. 1 cm. Some of non-productive fractures contain patches of highly electrically conductive spots. Data from coreholes K-33 and K-21 indicate that these fractures contain not interconnected cavities in their calcite or quartz fills, which became filled by drilling mud, providing an electrical image characterized by resistive mineral fill with scattered conductive patches. Similar image is usual for productive fractures at minor fluid entries. Cavities in their fills, however, form interconnected systems in this case. Major fracture-controlled fluid entries in well KRH 3-1 ST are characterized by increased complexity and density of electrically conductive spots within fractured interval, as seen at fluid entries at 2379.3-2380.5m and 2343.3-2344.2 m. Fractures at all fluid entries in well KRH 3-1 ST, irrespective of their fracture densities and the presence or absence of larger cavities, have one thing in common; relatively small average apertures, indicating that their permeability is controlled by a combination of aperture and interconnectivity.

Minor fluid entry at a depth of 2032.0 m in well KRH 2-1 OH allows to study a productive fault. Its displacement is sinistral and it has only moderate tendency to be reactivated in the present stress regime and only moderate tendency to dilate if reactivated. The fracture density at this entry is increased to 100 fractures per 10 m.

Because the slip and dilation tendencies of this fault range from 0.47-0.75, its permeability must be not solely stress-controlled, when compared to fracture-controlled fluid entries in the same well with slip/dilation tendencies approaching 1. Its FMS image indicates that fault is about 4.57 m thick and its core is sandwiched between two damage zones formed by numerous fractures, which cause a dramatically increased fracture density mentioned earlier. Image of the fault core contains resistive spots on a highly conductive background, indicating resistive andesite clasts surrounded by highly conductive either tectonic clay or porous matrix. These facts allow to conclude that not ideal dilation and slip tendencies of this fault seem to be evened up by its size and highly permeable damage zones.

The best productive fractures in well KRH 3-1 ST are sub-parallel to the quartz diorite dyke hosting the geothermal system and roughly perpendicular to the minimum compressive stress σ_3, which trends 98^{o}. Therefore, these fractures have tendency to achieve the maximum possible aperture.

Fluid entry at a depth of 2704.4 m in well KRH 3-1 ST documents that it is frequently an interplay of numerous fractures that controls a producing zone (**Tab. 5**). It is no so fracture density, as there is no density peak at the fluid entry in comparison to surrounding host rock. **Tab. 5** indicates, however, that the behavior of fractures below and above the entry is very different. Fractures below the entry have slip/dilation tendencies close to maximum. In contrast, fractures above the entry do not have slip/dilation tendencies considerably above the minimum. Consequently, they display a tendency to close and seal off the fluid flow, while fractures below have a tendency to keep their apertures close to maximum levels and facilitate flow. Similar relationships can be found controlling fluid entries at depths of 2267, 2337.5, 2355, 2827.5, 2863, 2910.5 and 3040 m in the same well. A similar stress control on fracture apertures has been recognized in numerous fracture systems worldwide (e.g., Carlsson and Olsson, 1979; Hancock, 1985; Barton et al., 1995; Fisher et al., 1996; Finkbeiner et al., 1997; Sigal, 1998, pers. com.; Caine, 1999).

4. 5. Reservoir character controls

As documented earlier, the reservoir seems to be in pressure communication (**Fig. 8b**). This would imply that there is sufficient permeability/connectivity to keep reservoir without compartments, if there were not geochemical evidences about several fluid and gas groups (**Fig. 9**). Thermal regime data (**Fig. 2b**) also indicate some complexity in the field, which can be divided into southern, i.e. Telaga Bodas, central and northern, i.e. Karaha, segments.

The central segment provides probably the most distinct evidences about the background conductive heat transfer regime, because it is located to the north of the dyke feeder, which supplies large amount of magmatic fluids and gasses though a chimney with fault and fracture clusters (**Fig. 10b**), and because it is located to the south of the region, where thermal regime is significantly perturbed by warm fluids ascending along numerous larger faults (**Fig. 1b, 10b**). Wells in the central segment are characterized by temperature/depth curves indicating dominant conductive regime in the upper portion of the section and fluid-dominated heat transfer below it (**Fig. 2a**). Clay-rich cap rock does not seem to be breached by any large faults, which helps the cap rock to maintain its thermal blanketing effect on the underlying reservoir (**Fig. 10b**). Fluid regime in the deeper reservoir in this segment indicates flow towards the south, towards the dyke feeder. The shallower reservoir contains a vapor zone.

The northern, Karaha, segment neither has its cap rock intact (**Fig. 1b**) nor its cap rock provides thermal blanketing for the underlying reservoir (**Fig. 10b**). Wells in this region indicate the ascent of geothermal fluids along fault zones/fracture clusters into the cap rock levels (**Fig. 10b**), where they change the thermal regime from conductive to convective (**Fig. 4a**). Breaching of the cap rock is further indicated by lost circulation zones recognized in cap rock levels in wells KRH 1-1, KRH 2-1, KRH 3-1, KRH 4-1, KRH 5-1 and K-10 (**Fig. 8a, 10b**). The ascent of geothermal fluids in the northern segment apparently provided a significant cooling mechanism, as it can be implied from a comparison of the top surface of the epidote mineralization and the present-day 250° C temperature surface (**Fig. 5b**). The northern segment underwent the most dramatic cooling of all three segments, definitely larger than conductive cooling in the central segment (**Fig. 5b**). Apart from geothermal fluids ascending along fault/fracture zones, the overall fluid regime in the deeper reservoir of the northern segment indicates fluid flow towards the south, towards the dyke feeder (**Fig. 10b**). The shallower reservoir contains a vapor zone (**Fig. 10b**).

The southern, Telaga Bodas, segment has its cap rock very thin and it is constantly warmed up by ascending geothermal fluids flowing to this region from the northern and central field segments and magmatic fluids and gases ascending from the dyke feeder (**Fig. 10b**). These two heat transport mechanisms help the southern segment to maintain relatively uncooled regime, as it can be implied from a comparison of the top surface of the epidote mineralization and the present-day 250° C temperature surface (**Fig. 5b**), where the total amount of cooling is rather minimal.

Despite of pressure communication in the whole field (Allis et al., 2000), geochemical data seems to indicate a series of convecting steam cells, each evaporating from and condensing into local pockets of brine. Each cell chemistry seems to be dictated by the Cl and B content of convecting steam (**Fig. 9b**). **Fig. 9b** indicates that most of the samples lie along a trend originating near the Cl/B trend defined by diorite and modified by addition of low Cl/B steam. Waters such as in well KRH 5-1 in the southern part of the field with distinct faults can be understood as reservoir fluids with added low Cl/B steam resulting in more dilute brines. Fluid composition in deep reservoir in the well KRH 3-1 ST can be explained as addition of high Cl/B steam to reservoir fluid. Relatively conservative alkali elements Rb, Li and Cs show a similar Rb loss relative to silicic volcanic reservoir rock (**Fig. 9a**) and their rough grouping indicates roughly the same origin, however, modified by geochemical changes driven by local convecting steam cells mentioned earlier. The apparent lack of equilibration among certain gases (**Fig. 9c**) indicates local influence. For example, the higher CH_4 and NH_3 contents indicate likely breakdown of organic matter. One of the wells with higher CH_4 content, well K-33, did penetrate lacustrine sediments (those dated in **Fig. 8b**) with higher organic content. Data from some other wells in the northern, Karaha, segment indicate penetration of sediments, probably deposited in small local lakes (**Joe helps with citing specific wells**). Increased H_2S content, since local temperatures are too high for bacterial origin, indicates magmatic source of fluids and gases in the southern, Telaga-Bodas, segment, which is in accordance with location of the dyke feeder (**Fig. 10b**) and indications provided by $\delta^{18}O$ and δD isotopes (Powell et al., 2001).

5. Conclusions

1) Critically-stressed ideally oriented fractures with high densities in the fracture reservoir can be made up for by faults of less ideal orientations because of their size advantage.
2) The reservoir also contains matrix-controlled production zones, which are located in tuff and sediment horizons.
3) The initial cap rock base was controlled by a combination of the a) initial mechanic stratigraphy and b) zoning of the penetrative alteration, further modified by a change from upper strike-slip to lower normal-fault stress regime controlling the fracture permeability of the reservoir.
4) Deepening of the cap rock base was controlled by downward fracture cementation by downward percolating condensate.
5) The lowermost reservoir bottom is controlled by a sharp brittle/ductile boundary located mostly within the quartz diorite dyke.
6) The effective reservoir bottom is controlled by a fuzzy boundary between open and closed fractures. This fracture behavior is controlled by the interplay of the normal stress resolved on fractures and the compressional strength of the wall rock. This interplay causes closing of fractures with different orientations at different depths.
7) Liquid reservoir zone is under-pressured by about 30 bar in comparison to cold hydrostatic column beneath surrounding valley floors, indicating its partially vapor-dominated regime.
8) Liquid zone pressure uniformity indicates good reservoir communication.
9) Fluid and gas chemistries in the reservoir vary due to both local sources and modification by local steam convection cells.

Acknowledgments

MN, JNM, GDN and RA were supported by DOE Grants to EGI (DE-FG07-00ID13892, 01-0059-5000-55900160 and 01-0059-5000-55800164). The managements and staff of the Karaha Bodas Company are thanked for providing data for this research.